Applied Catalysis B: Environmental 218 (2017) 111–118

Contents lists available at ScienceDirect

Applied Catalysis B: Environmental

journal homepage: www.elsevier.com/locate/apcatb

Bi quantum dots on rutile TiO_2 as hole trapping centers for efficient photocatalytic bromate reduction under visible light illumination

Jun Xiao[a,b], Weiyi Yang[a], Qi Li[a,*]

[a] Environment Functional Materials Division, Shenyang National Laboratory for Materials Science, Institute of Metal Research, Chinese Academy of Sciences, Shenyang, 110016, PR China
[b] University of Chinese Academy of Sciences, Beijing 100049, PR China

ARTICLE INFO

Article history:
Received 24 November 2016
Received in revised form 24 February 2017
Accepted 29 March 2017
Available online 16 June 2017

Keywords:
Bi quantum dots
Photocatalytic bromate reduction
Visible light
Hole trapping/consumption center
Charge carrier separation

ABSTRACT

Bi quantum dots were deposited onto rutile TiO_2 nanoparticles by a one-pot, solvent-thermal process to create the Bi/TiO_2 (rutile) heterojunction photocatalyst. Due to the specific semimetal property of Bi, a metal to semiconductor transition occurred for Bi quantum dots, which endowed them with the hole trapping capability to enhance the charge carrier separation in rutile TiO_2 and eliminate the need of sacrificial agents for the consumption of photogenerated holes in photocatalytic reduction process. The Bi/TiO_2 (rutile) heterojunction photocatalyst demonstrated an efficient photocatalytic bromate reduction under visible light illumination without the addition of sacrificial agents in the reaction solution, and it could be easily regenerated for reuse. Different with previously reported noble/transition metal modifications as the electron trapping center, this study demonstrated a novel material design strategy of the introduction of hole trapping centers to create photocatalysts with strong photocatalytic reduction capabilities, which could be readily adopted for a broad range of technical applications.

1. Introduction

As identified by the International Agency for Research on Cancer (IARC) as a 2 B substance (a possible carcinogen to humans) [1], the presence of bromate in drinking water from the ozonation disinfection is strictly regulated. The World Health Organization (WHO) suggested that the maximum contaminant level (MCL) of bromate in drinking water should not be over 10 $\mu g/L^{-1}$, and this standard has been adopted by many countries [2]. Various treatment technologies had been developed for the removal of bromate from drinking water, including physical adsorption [3], chemical reductions [4], and biological technologies [5]. However, their high cost, long treatment time, strict reaction conditions, and production of secondary pollutants limited their application in water treatment practice [6]. Thus, novel approaches should be developed for the removal of bromate from drinking water with high efficiency, economic feasibility, and environmental friendliness.

Since the pioneer work of Fujishima and Honda in 1972 [7], TiO_2 phtotocatalyst has been attracting great research attentions due to its potential in solar energy conversion/storage for various applications [8]. When TiO_2 is excited, both reduction and oxidation reactions could happen when photogenerated electrons and holes migrate to its surface and react with substances absorbed on/near its surface [9]. Photocatalytic reduction could provide promising solutions to hydrogen production from water splitting, CO_2 reduction for fuel production, and the removal of various environmental pollutants [10,11]. It had demonstrated that photocatalysis could be a promising technology for the removal of aqueous oxoanions from drinking water [12]. However, previous studies on the photocatalytic bromate reduction were usually conducted under UV light illumination [2,12,13], or had limited photocatalytic reduction efficiency [1,14]. To enhance the photocatalytic reduction efficiency, sacrificial agents are usually needed to deplete the photogenerated holes [12,15,16]. However, it could increase the complexity and cost of the operation, and may not be appropriate for drinking water treatment due to the addition of substances with potential hazard.

For the enhancement of the photocatalytic efficiency, noble/transition metal modification is widely used as the electron trapping center to enhance the photogenerated electron-hole pair separation due to their relatively high work functions [17–19]. However, this material design strategy could not deplete photogenerated holes with strong oxidation capability, and the addition of sacrificial agents is still needed for the efficient photocatalytic reduction. It would be most desirable to design a photocatalyst

* Corresponding author at: 72 Wenhua Road, Shenyang, Liaoning Province, 110016, PR China.
E-mail addresses: qili@imr.ac.cn, qiliuiuc@gmail.com (Q. Li).

http://dx.doi.org/10.1016/j.apcatb.2017.03.084
0926-3373/

system for photocatalytic reduction in which the charge carrier recombination could be minimized by modifications with hole trapping and consumption capability. Thus, the addition of sacrificial agents could be removed to solve problems associated with it. As a semimetal element (a weak overlap exists between its valence and conduction bands), bismuth may provide the hole trapping and consumption capability. Unlike most metals, bulk Bi has a relatively low work function of ~4.22 eV [20], close to that of TiO_2 at ~4.20 eV [21]. With its size decrease into the nano range, the quantum confinement could induce a transition from metal to semiconductor on Bi with the moving up of its conduction subbands and moving down of its valence subbands [22]. So photogenerated electrons could not transfer from TiO_2 to Bi quantum dots anymore, while photogenerated holes could transfer from TiO_2 to Bi quantum dots and be consumed by oxidizing Bi^0 to Bi^{3+}. Thus, it could enhance the lifetime of photogenerated electrons for an efficient reduction process, while no sacrificial agents are needed to deplete holes. Although several Bi-modified semiconductor photocatalysts had recently been reported in literature, including Bi/TiO_2 [23], Bi/BiOCl [24], Bi/$(BiO)_2CO_3$ [25], and Bi/Bi_2O_3 [26], they relied on the traditional electron trapping or plasmonic function of Bi as a transition metal, which could not trap/consume holes for an enhanced photocatalytic reduction.

Compared with commonly used anatase TiO_2, rutile TiO_2 has a relatively smaller bandgap of ~3.0 eV, beneficial for the visible light absorption and subsequent photocatalytic activity under visible light illumination if its intrinsic fast recombination rate of photogenerated electron and hole pairs could be suppressed [27]. In this study, we developed a one-pot, solvent-thermal process to synthesize the Bi/TiO_2 (rutile) heterojunction photocatalyst. It demonstrated a superior photocatalytic reduction of bromate without the addition of sacrificial agents under visible light illumination, which could be attributed to the dual modification effects of Bi quantum dots on both the enhanced charge carrier separation and the trapping/consumption of holes.

2. Experimental

2.1. Materials and chemicals

All chemicals were of analytical grade and were used without further purification. Degussa P25 TiO_2 nanoparticles and rutile TiO_2 nanoparticles were purchased from Aladdin Industrial Corporation (Shanghai, P. R. China). SiO_2 was purchased from Qingdao Haiyang Chemical Corporation (Qingdao, P. R. China). Ethylene glycol, polyvinylpyrrolidone (PVP, K-30), bismuth nitrate pentahydrate, sodium bromate and $HAuCl_4{\cdot}3H_2O$ were purchased from Sinopharm Chemical Reagent Corporation (Shanghai, P. R. China). Deionized (DI) water (18.2 MΩ) was produced by an ultrapure water system.

2.2. Synthesis of photocatalysts

In a typical synthesis process, 1 mL 10 M HNO_3 and 9 mL DI water were added into 50 mL ethylene glycol under continuous stirring. Then, 0.061 g $Bi(NO_3){\cdot}5H_2O$ and 1 g PVP (K-30) were added into this solution successively, and the solution was stirred continuously to ensure that all reagents were dissolved. After the solution became transparent, 1 g rutile TiO_2 nanoparticles were dispersed into the solution with the molar ratio of Bi/Ti at 1%, and the mixture was stirred for another 30 min to ensure the good dispersity of these rutile TiO_2 nanoparticles before it was transferred into a 50 mL Teflon-lined stainless steel autoclave. The solvent-thermal process was conducted at 160 °C for 24 h. After the reaction, the precipitate was centrifuged, washed several times with ethanol and DI water, respectively, and then dried at 60 °C in vacuum for 12 h to obtain the final product of the Bi(1.0)/rutile TiO_2 photocatalyst. For comparison purpose, the Bi(1.0)/SiO_2 sample, the Bi(1.0)/P25 TiO_2 photocatalyst and the Au(1.0)/rutile TiO_2 photocatalyst were also prepared by the similar solvent-thermal process. For the Bi(1.0)/SiO_2 sample, Bi(1.0)/P25 TiO_2 photocatalyst, SiO_2 nanoparticles and P25 TiO_2 nanoparticles were used to replace rutile TiO_2 nanoparticles, respectively, while $HAuCl_4{\cdot}3H_2O$ was used to replace $Bi(NO_3){\cdot}5H_2O$ to obtain the Au(1.0)/rutile TiO_2 photocatalyst. Pure Bi nanoparticles were prepared by a hydrothermal synthesis method as previously reported [28]. The Bi_2O_3(1.0)/rutile TiO_2 photocatalyst was prepared by the calcination of the Bi(1.0)/rutile TiO_2 photocatalyst at 400 °C for 2 h in air.

2.3. Characterization of photocatalysts

The crystal structures of samples were obtained by X-ray diffraction (XRD) on a D/MAX-2004 X-ray powder diffractometer (Rigaku Corporation, Tokyo, Japan) with Ni-filtered Cu Kα (λ = 1.54178 Å) radiation at 56 kV and 182 mA. The sample morphology and selected area electron diffraction pattern were obtained on a JEOL 2100 transmission electron microscope (JEOL Ltd, Tokyo, Japan) operating at 200 kV. EDX spectrum measurement was conducted by a Model SUPRA55 SEM system (Zeiss, Germany) equipped with energy dispersive spectrometer. X-ray photoelectron spectroscopy (XPS) measurements were conducted on an ESCALAB 250 X-ray photoelectron spectrometer (Thermo Fisher Scientific Inc., Waltham, MA, U.S.A.) with an Al K anode (1486.6 eV photon energy, 300 W). The UV–vis spectra of samples were measured on a UV-2550 spectrophotometer (Shimadzu Corporation, Kyoto, Japan). The surface photovoltage spectra (SPS) of samples were measured with a home-built apparatus [29]. The Bi content in the Bi(1.0)/TiO_2 (rutile) catalyst was determined with an inductively coupled plasma mass- spectrometer (Perkin Elmer −SCIEX ELAN DRCe ICP-MS, Norwalk, CT, USA).

2.4. Photocatalytic reduction of bromate under visible light illumination

In this study, bromate was chosen as a model pollutant to evaluate the photocatalytic reduction performances of different photocatalysts under visible light illumination. In a typical experiment, 40 mg photocatalyst was loaded into a glass beaker, which contained 80 mL aqueous bromate solution (10 mg/L). A 300-W xenon lamp (PLSSXE300, Beijing Perfect Light Technology Co., Ltd., Beijing, P. R. China) was used as the light source, which had a glass filter to provide zero light intensity below 400 nm. Before the photocatalytic treatment, the suspension was magnetically stirred in dark for 0.5 h to reach the adsorption/desorption equilibrium. At each time interval, 5 mL suspension was withdrawn and the photocatalyst was separated by centrifugation at 10,000 rpm for 5 min. The concentrations of bromate and bromide in the supernatant solution were analyzed by ion chromatography (Dionex ICS 1100 Ion Chromatograph with a conductivity cell).

3. Results and discussion

3.1. Material design for efficient photocatalytic reduction without the addition of sacrificial agents

The deposition of Bi quantum dots on rutile TiO_2 nanoparticles is the key in our material design for highly efficient photocatalytic reduction under visible light illumination. Fig. 1a and b shows the energy band alignment diagrams for rutile TiO_2/bulk Bi and rutile TiO_2/Bi quantum dots, respectively. The conduction band (CB) bottom and valence band (VB) maximum of rutile TiO_2 are ~−0.59

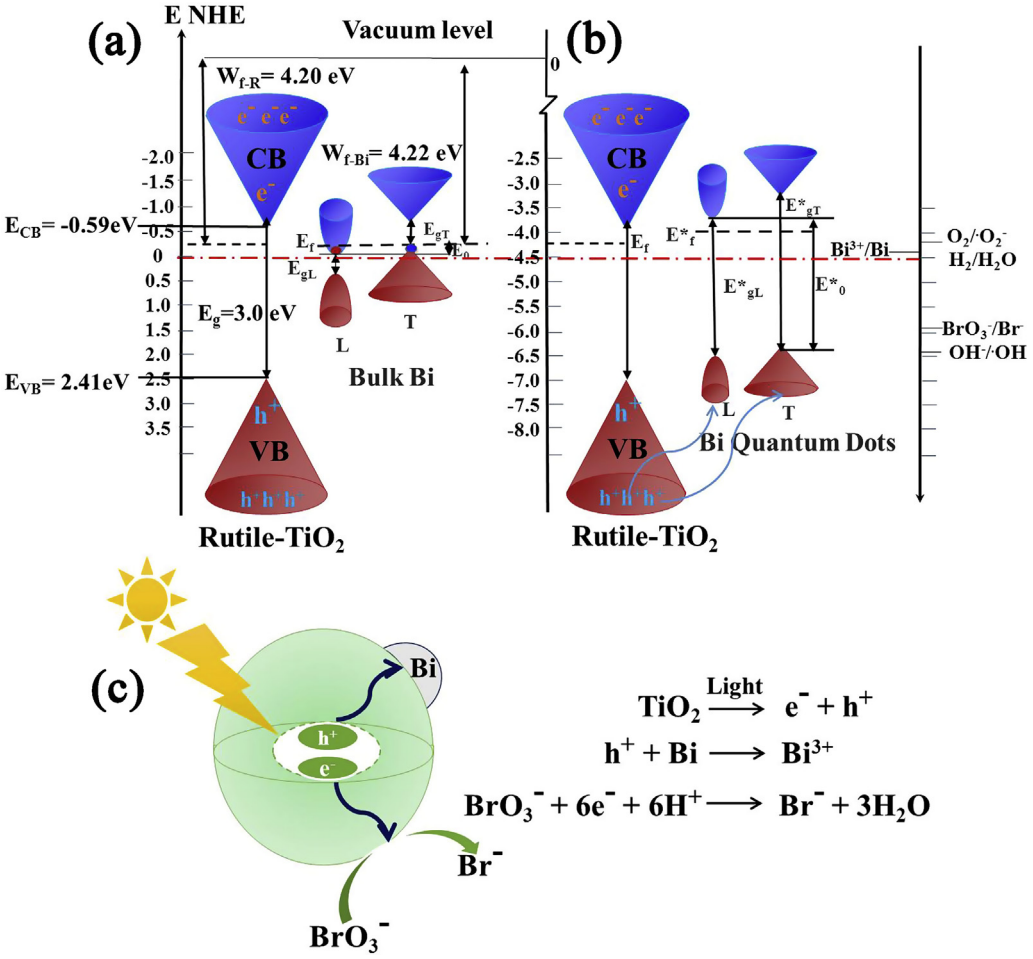

Fig 1. Proposed energy band structures of (a) Bulk Bi/TiO_2 (rutile) and (b) the Bi(1.0)/TiO_2 (rutile) photocatalysts. (c) The photocatalytic activity enhancement mechanism under visible light illumination. (Note: E_f refers to Fermi energy, E_{gL} refers to gap energy at L-point of the Brillouin zone, E_{gT} refers to energy gap at T-point of the Brillouin zone, and E_0 refers to energy difference between the bottom of the conduction band at the L-point of the Brillouin zone and the top of the valence band at the T-point of the Brillouin zone.).

and 2.41 eV, respectively [30,31], and its work function is ~4.20 eV [21]. For metallic bulk Bi, its work function is ~4.22 eV [20]. Thus, photoexcited electrons could flow from rutile TiO_2 to bulk Bi (see Fig. 1a), similar to other reported noble/transition metal modifications as electron trapping centers. When Bi quantum dots are loaded on rutile nanoparticles, however, the specific semimetal property of Bi could create a different situation as demonstrated in Fig. 1b. As previously reported, the conduction subbands of Bi move up in the band energy diagram as its size decreases, while its valence subbands move down accordingly, inducing a metal to semiconductor transition for Bi [22,32]. Therefore, the Fermi level of Bi quantum dots would be promoted (see Fig. 1b), and photogenerated electrons by rutile TiO_2 under visible light illumination could not transfer from rutile TiO_2 to Bi quantum dots. Instead, they must remain on rutile TiO_2 nanoparticles, while photogenerated holes could migrate to Bi quantum dots. Thus, Bi quantum dots should serve as the hole trapping center in the Bi(1.0)/TiO_2 (rutile) photocatalyst, which could also enhance the separation of photogenerated electron-hole pairs. The redox potentials of $O_2/{}^{\bullet}O_2^-$, $OH^-/{}^{\bullet}OH$, BrO_3^-/Br^-, and Bi^{3+}/Bi are ~ −0.33 eV, 1.99 eV, 1.423 eV and 0.2 eV, respectively [21,33]. Therefore, photogenerated electrons would prefer to reduce bromate to bromide, while photogenerated holes would prefer to oxidize Bi to Bi^{3+} after their production and separation (see Fig. 1c). Thus, no additional sacrificial agents are needed to scavenge photogenerated holes for highly efficient photocatalytic reduction under visible light illumination because of the role of Bi as a hole trap.

3.2. Crystal structure and morphology of the Bi(1.0)/TiO_2 (rutile) photocatalyst

Fig. 2a shows the XRD pattern of the Bi(1.0)/TiO_2 (rutile) photocatalyst, compared with that of the commercial rutile TiO_2 nanoparticles. After the deposition of Bi (1% molar percentage of Ti), the XRD diffraction peaks of the Bi(1.0)/TiO_2 (rutile) photocatalyst still belonged to the rutile TiO_2 phase (PDF Card No. 21-1276), and no obvious XRD diffraction peak of Bi was observed. This observation may be attributed to the low content and high dispersion of deposited Bi quantum dots, and similar results had been reported in various metal/semiconductor composite photocatalysts [25,34]. Fig. 2b shows the TEM observation of the Bi(1.0)/TiO_2 (rutile) photocatalyst, which clearly demonstrated that dark Bi quantum dots with the size of several nm were dispersed on rutile TiO_2 nanoparticles. Insert images in Fig. 2b show the corresponding selected area electron diffraction (SAED) pattern of the sample, which demonstrated that these rutile TiO_2 nanopaticles had a high degree of crystallinity. Continuous sharp circles with *d*-spacing of 0.325, 0.245, 0.215, and 0.169 nm could be clearly identified, which corresponded to (110), (101), (111), and (211) lattice planes of rutile TiO_2, respectively. In addition, two diffraction spots with the *d*-spacing of 0.395 nm could also be observed in the SAED pattern

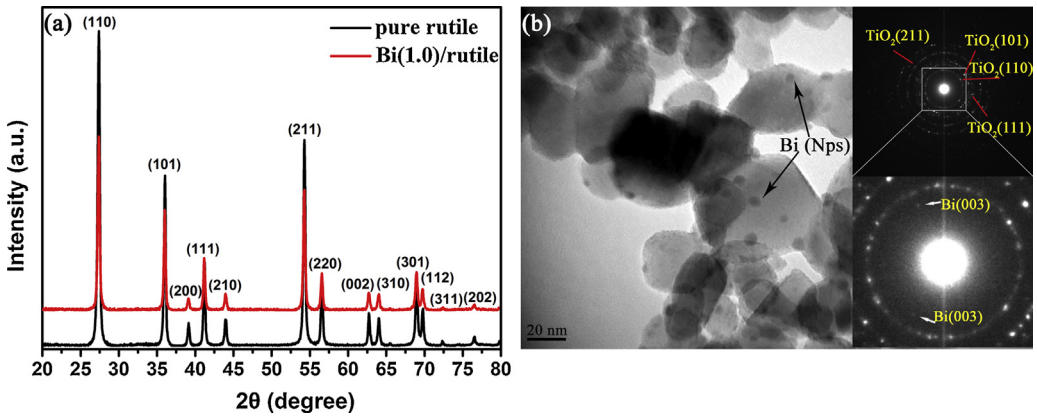

Fig. 2. (a) XRD patterns of the Bi(1.0)/TiO_2 (rutile) photocatalyst and rutile TiO_2 nanoparticles. (b) TEM image of the Bi(1.0)/TiO_2 (rutile) photocatalyst (Note: Insert images show the SAED patterns).

(see the insert image in the right bottom of Fig. 2b), which could be attributed to the (003) lattice plane of the rhombohedral phase of elemental Bi (PDF Card No. 44–1246).

3.3. Chemical composition of the Bi(1.0)/TiO_2 (rutile) photocatalyst

ICP-MS measurement result showed that the Bi/Ti atomic ratio in the Bi(1.0)/TiO_2 (rutile) photocatalyst was ~0.89%, which was close to that in the reaction solution. To further examine the existence and state of Bi species in the Bi(1.0)/TiO_2 (rutile) photocatalyst, XPS investigation was conducted to obtain the semi-quantitative data on its composition. Fig. 3a shows the representative XPS survey spectrum of the Bi(1.0)/TiO_2 (rutile) photocatalyst, which demonstrated clearly the existence of Ti, O, and Bi in the sample. Fig. 3b shows the high resolution XPS scan over Bi 4*f* peaks, in which both metallic Bi^0 and oxidized Bi^{3+} states could be observed. The two XPS peaks at 156.9 and 162.3 eV could be assigned to Bi^0 $4f_{7/2}$ and Bi^0 $4f_{5/2}$ [35], while the two XPS peaks at 159.1 and 164.4 eV could be assigned to Bi^{3+} $4f_{7/2}$ and Bi^{3+} $4f_{5/2}$ [36]. Similar observation had been reported by Dong et al. [37], which could be attributed to the easy surface oxidation of Bi element in air to form a thin layer of Bi_2O_3. Fig. 3c shows the high resolution XPS scans over Ti 2*p* peaks. The two XPS peaks at 458.6 eV and 464.7 eV could be assigned to Ti^{4+} $2p_{3/2}$ and Ti^{4+} $2p_{1/2}$ [38].

As a surface characterization technique, XPS could determine the surface composition ratio within a very shallow depth. The XPS analysis results showed that the surface Bi/Ti atomic ratio was ~3%, higher than the overall Bi/Ti atomic ratio in the Bi(1.0)/TiO_2 (rutile) photocatalyst determined by ICP-MS. This result was consistent with the fact that Bi was deposited on the surface of rutile TiO_2. Fig. S1 in the supplementary material shows the EDX spectrum and the corresponding elemental mapping results of the Bi(1.0)/TiO_2 (rutile) photocatalyst. It demonstrated that Bi distributed relatively uniformly in the sample. The surface Bi/Ti atomic ratio was determined at ~2.5% by the EDX analysis, which was close to the XPS analysis result. Thus, TEM and the sample composition analysis results clearly demonstrated that well dispersed metallic Bi quantum dots were loaded on the surface of rutile TiO_2 nanoparticles to create the designed Bi/TiO_2 (rutile) heterojunction photocatalyst.

3.4. Optical properties of the Bi(1.0)/TiO_2 (rutile) photocatalyst

The optical properties of the Bi(1.0)/TiO_2 (rutile) photocatalyst were examined by measuring its UV–vis diffuse reflectance spectrum. From the reflectance data, optical absorbance could be approximated by the Kubelka-Munk function [39]. Fig. 4 shows the light absorbance of the Bi(1.0)/TiO_2 (rutile) photocatalyst, compared with that of the commercially available Degussa P25 TiO_2 nanoparticles and the rutile TiO_2 nanoparticles. The insert image in Fig. 4 shows their band gap values, which were determined by the construction of Tauc Plots ($(F(R)^*hv)^n$ vs. hv) from their light absorbance data [39]. Degussa P25 TiO_2 nanoparticles demonstrated the characteristic spectrum with the fundamental absorbance stopping edge at ~400 nm, and the corresponding band gap was determined at ~3.17 eV. The rutile TiO_2 nanoparticles demonstrated an obvious light absorption in the visible light region with the absorbance stopping edge at ~ 420 nm, and the corresponding band gap was determined at ~3.0 eV. Compared with that of the rutile TiO_2 nanoparticles, no obvious change was observed on the main light absorbance of the Bi(1.0)/TiO_2 (rutile) photocatalyst after being loaded with Bi quantum dots. The band gap of the Bi(1.0)/TiO_2 (rutile) photocatalyst was almost the same as that of the rutile TiO_2 nanoparticles. A clear absorption tail was observed for the light absorbance of the Bi(1.0)/TiO_2 (rutile) photocatalyst, which could be attributed to localized surface plasmon effect from Bi quantum dots and did not change the main light absorption from the rutile TiO_2 [40].

3.5. Photocatalytic reduction of bromate by the Bi(1.0)/TiO_2 photocatalyst under visible light illumination

The photocatalytic reduction activity of the Bi(1.0)/TiO_2 photocatalyst was demonstrated by its bromate reduction performance under visible light illumination without the addition of sacrificial agents. Fig. 5a shows the bromate photocatalytic reduction result by the Bi(1.0)/TiO_2 (rutile) photocatalyst under visible light illumination. During the photocatalytic reduction process, the bromate concentration decreased continuously, while the bromide concentration gradually increased. After ~60 min reaction, the bromate concentration dropped from ~0.078 mmol/L (10 ppm) to zero, representing a 100% conversion ratio. The sum of bromate and bromide concentrations during the photocatalytic reduction process was very close to the initial bromate concentration, which indicated that bromide was the only photocatalytic reduction product in the present study. The photocatalytic bromate reduction data could be best fitted by the pseud-first-order kinetic model ($R^2 = 0.978$), and the K_{obs} was determined from the experimental data fitting as 0.064 min^{-1}.

To verify the effects of various components in the Bi(1.0)/TiO_2 photocatalyst, comparison experiments were conducted. Fig. 5b compares the residue bromate concentration versus treatment time by pure Bi nanoparticles, the Bi(1.0)/SiO_2 sample, the Bi_2O_3(1.0)/TiO_2 (rutile) photocatalyst, and the Bi(1.0)/rutile photo-

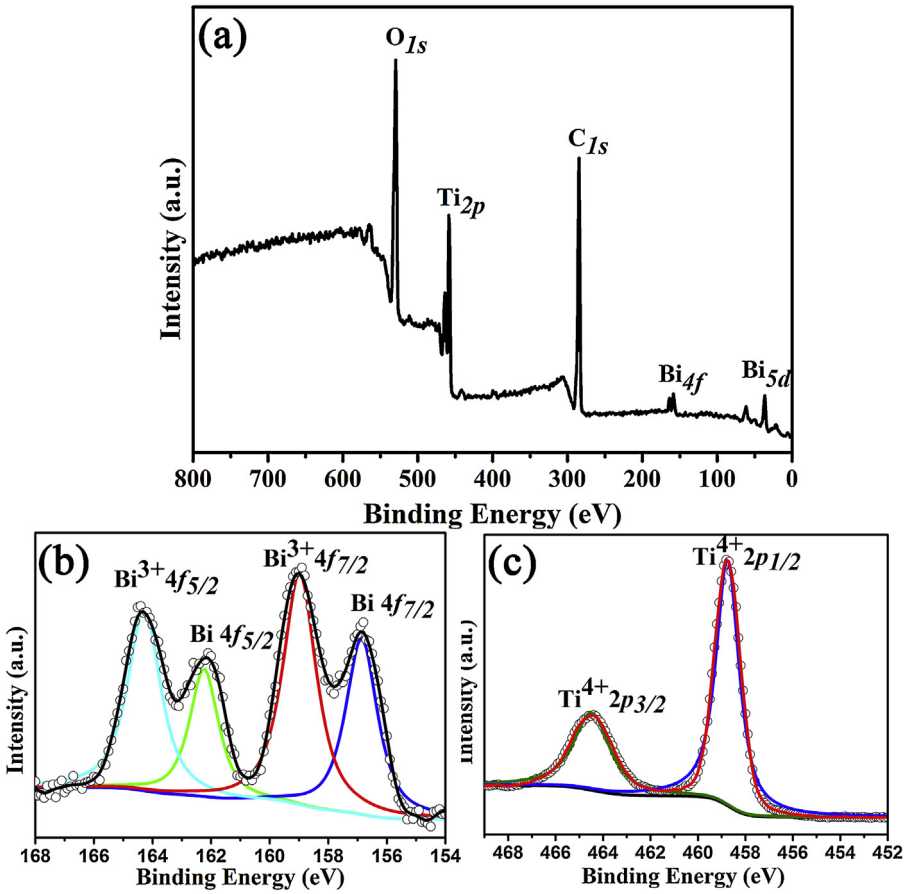

Fig. 3. (a) XPS survey spectrum of the Bi(1.0)/TiO_2 (rutile) photocatalyst. (b) The high resolution XPS scans over Bi 4*f* peaks. (c) The high resolution XPS scans over Ti 2*p* peaks.

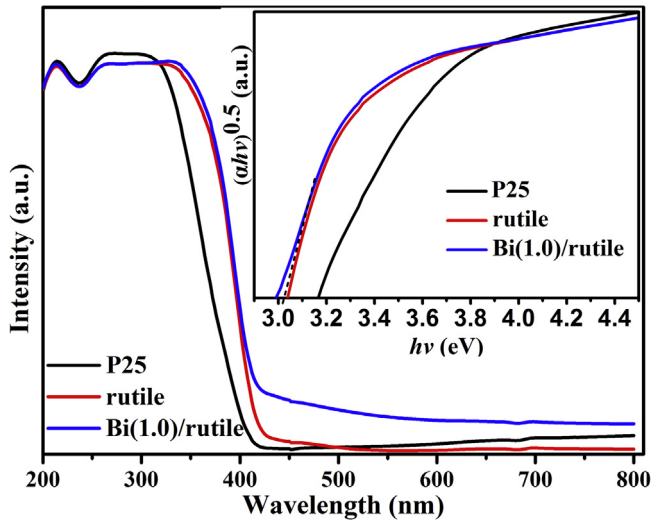

Fig. 4. UV–vis light absorbance spectra of the Bi(1.0)/TiO_2 (rutile) photocatalyst, Degussa P25 TiO_2 nanoparticles, and the rutile TiO_2 nanoparticles (Note: Insert image shows their Tauc plots).

catalyst under visible light illumination. Both pure Bi nanoparticles and the Bi(1.0)/SiO_2 sample had no bromate reduction capability, which suggested that the fast photocatalytic bromate reduction by the Bi(1.0)/TiO_2 (rutile) photocatalyst was not from Bi quantum dots themselves. After even 2 h visible light illumination, the Bi_2O_3(1.0)/TiO_2 (rutile) photocatalyst could only reduce ~44% bromate, which was much worse than that by the Bi(1.0)/TiO_2 (rutile) photocatalyst. This observation suggested that the electron-trapping Bi_2O_3 could not compete with hole-trapping Bi on the enhancement of photocatalytic reduction process, indicating that the thin layer of Bi_2O_3 on Bi quantum dots could not play an important role in the efficient bromate photocatalytic reduction by the Bi(1.0)/TiO_2 (rutile) photocatalyst. Thus, the fast photocatalytic bromate reduction by the Bi(1.0)/TiO_2 (rutile) photocatalyst should from the interaction between rutile TiO_2 and Bi quantum dots as we proposed.

Fig. 5c compares the residue bromate concentration versus treatment time under different conditions. Without photocatalyst presence, no obvious changes were observed on the bromate con-centration after 2 h visible light illumination, indicating that the bromate concentration decrease observed in its photocatalytic reduction process could not be caused by visible light illumination alone. The adsorption of bromate onto the Bi(1.0)/TiO_2 (rutile) photocatalyst in dark was also examined, which demonstrated that its adsorption was minimal. When rutile TiO_2 nanoparticles and P25 TiO_2 nanoparticles were used, the bromate concentration dropped ~20% (rutile) and ~60% (P25) after 2 h visible light illumination, respectively, while more visible light could be absorbed by rutile TiO_2 nanoparticles than P25 TiO_2 nanoparticles. It is well known that rutile TiO_2 is usually less active because of its fast electron-hole pair recombination rate [41], while electron-hole pair separation could be enhanced for P25 TiO_2 nanoparticles due to the well-known mixed phase effect of P25 with the co-existence of anatase and rutile phases [42]. This observation clearly demonstrated the importance of electron-hole separation to obtain a good photocatalytic performance. After being deposited with Bi quantum dots, however, the Bi(1.0)/TiO_2 (rutile) photocatalyst had a much better performance than the Bi(1.0)/P25 photocatalyst. For a complete removal of bromate in the solution, it only

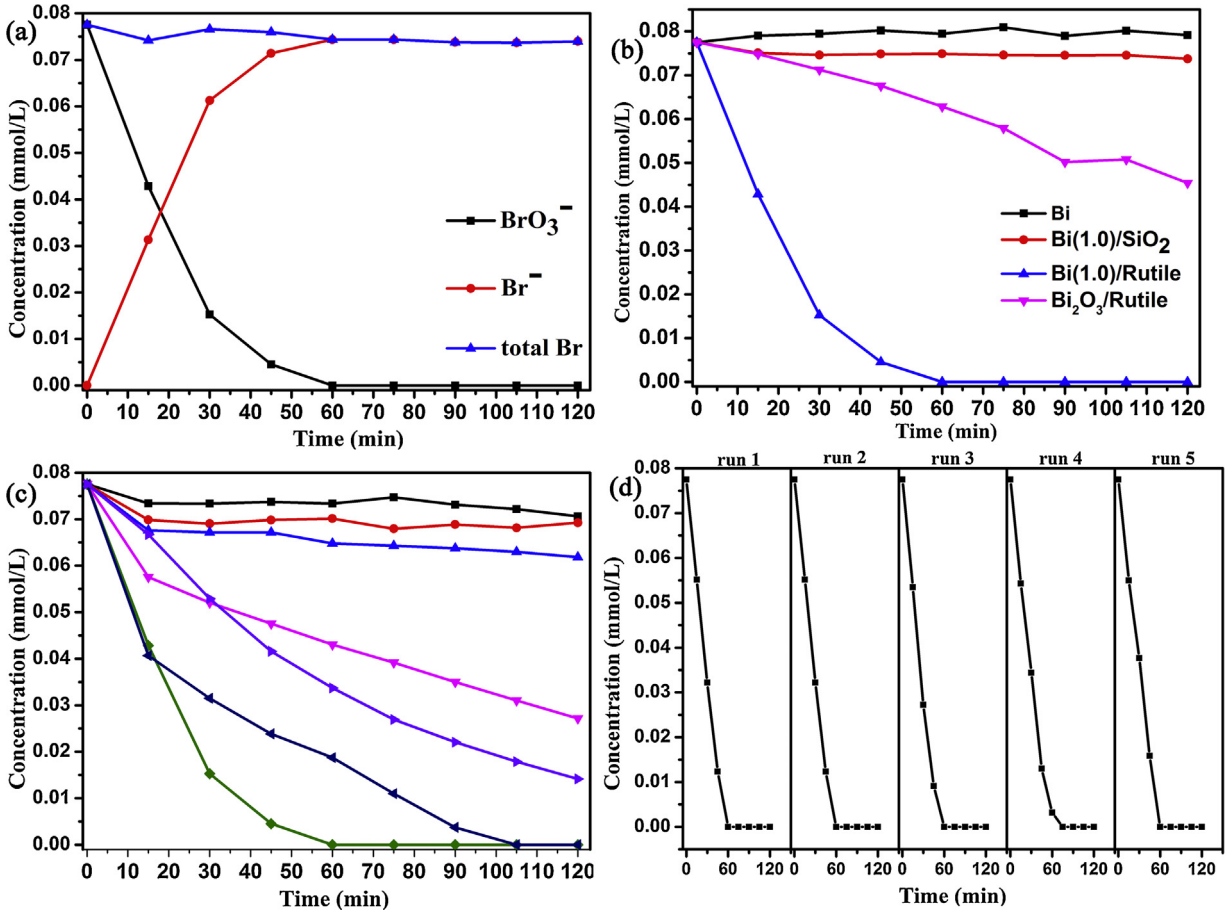

Fig. 5. (a) The bromate photocatalytic reduction result by the Bi(1.0)/TiO_2 (rutile) photocatalyst under visible light illumination (initial bromate concentration of 10 ppm, pH = 7, catalyst loading of 0.5 g L^{-1}). (b) The residue bromate concentration versus treatment time by pure Bi nanoparticles, the Bi(1.0)/SiO_2 sample, Bi_2O_3(1.0)/TiO_2 (rutile) and the Bi(1.0)/TiO_2 (rutile) photocatalyst under visible light illumination. (c) The residue bromate concentration versus treatment time under different conditions (black line: only light, red line: Bi(1.0)/TiO_2 (rutile) in dark, blue line: rutile with light, pink line: P25 with light, purple line: Au(1.0)/TiO_2 (rutile) with light, dark blue line: Bi(1.0)/P25 with light, and green line: Bi(1.0)/TiO_2 (rutile) with light). (d) The bromate photocatalytic reduction by the Bi(1.0)/TiO_2 (rutile) photocatalyst under visible light illumination for five runs. (For interpretation of the references to colour in this figure legend, the reader is referred to the web version of this article.)

took ~60 min for the Bi(1.0)/TiO_2 (rutile) photocatalyst, while it took ~105 min for the Bi(1.0)/P25 photocatalyst. These observations suggested that the electron-hole separation effect of Bi quantum dots prevailed, and the observed better bromate photocatalytic reduction by the Bi(1.0)/TiO_2 (rutile) photocatalyst than the Bi(1.0)/P25 photocatalyst should be attributed to the better visible light absorption of rutile TiO_2 than that of P25 TiO_2. Thus, rutile TiO_2 could serve as a highly efficient photocatalyst with the deposition of Bi quantum dots. The photocatalytic bromate reduction by the Au(1.0)/TiO_2 (rutile) photocatalyst was also examined under visible light illumination, which was a typical noble metal-modified TiO_2 photocatalyst. It demonstrated a much worse bromate photocatalytic reduction performance than the Bi(1.0)/TiO_2 (rutile) photocatalyst, which clearly demonstrated that the creation of hole trapping centers by the deposition of Bi quantum dots in our material design could have a superior photocatalytic reduction capability than the creation of electron trapping centers by the deposition of noble/transition metal modifications.

Fig. 5d shows the bromate photocatalytic reduction by the Bi(1.0)/TiO_2 (rutile) photocatalyst under visible light illumination for five runs. After each run, the photocatalyst was collected, washed, reduced by ethylene glycol, and then reused for the next run. Unlike the consumed sacrificial agents, the Bi(1.0)/TiO_2 (rutile) photocatalyst demonstrated a good regeneration capability and reusability. Similar bromate photocatalytic reduction behavior and no obvious efficiency loss were observed for the five runs in general. Fig. S2 in the supplementary material shows the TEM observations of the photocatalyst before and after the bromate photocatalytic reduction for five runs. No obvious morphology changes could be observed, which also indicated its good regeneration capability and reusability.

3.6. Hole trapping and consumption by Bi quantum dots

To verify the hole trapping and consumption role of Bi quantum dots in the Bi(0.1)/TiO_2 (rutile) photocatalyst, the Bi chemical state change under visible light illumination was examined by XPS analysis. Fig. 6a shows the high resolution XPS scans over Bi 4*f* peaks for different visible light illumination time, which clearly demonstrated that the ratio between Bi^{3+}/Bi^0 increased from ~1.314:1 to 2.986:1 with the illumination time increase to 2 h. This observation suggested that Bi^0 was gradually oxidized to Bi^{3+} under visible light illumination, which could be attributed to the trapping and consumption of photogenerated holes by these Bi quantum dots. The Ti chemical state change under visible light illumination was also examined by XPS analysis. Fig. 6b shows the high resolution XPS scans over Ti 2*p* peaks before and after visible light illumination. It could be found that part of Ti^{4+} was reduced to Ti^{3+} after visible light illumination, which should come from the excess of photoexcited electrons on TiO_2 surface due to the consumption of photoexcited holes by Bi quantum dots. The surface photovoltage spectrum (SPS) measurement was conducted to investigate the photoinduced car-

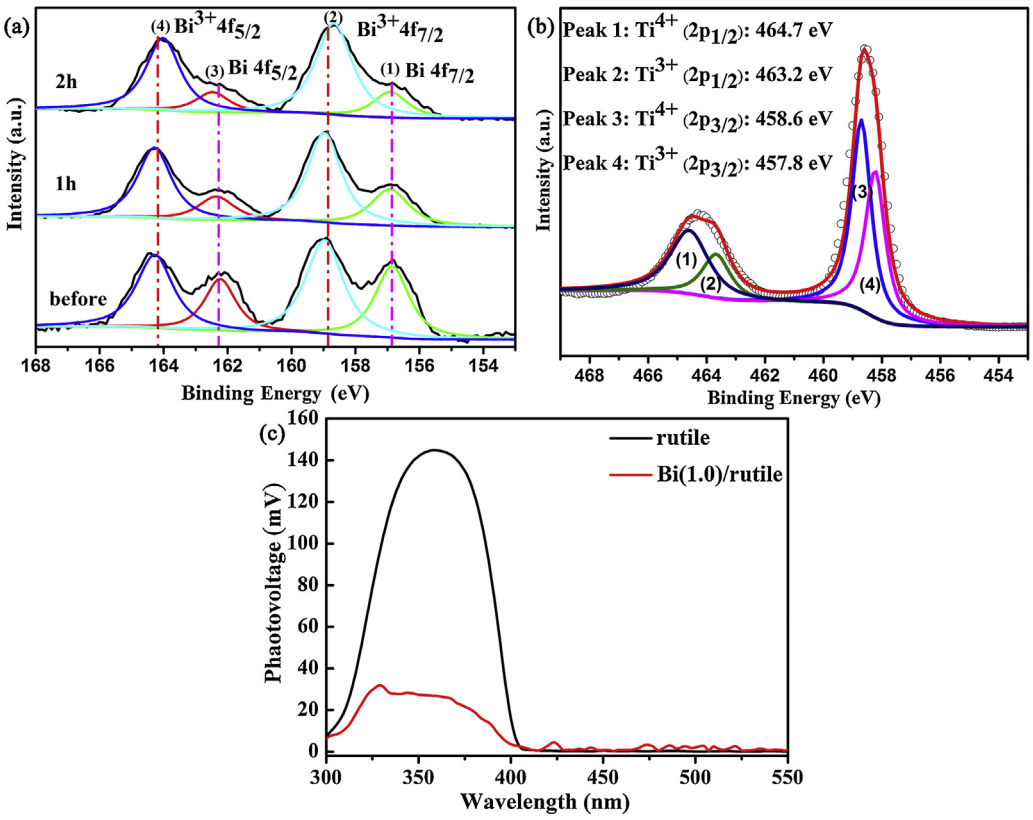

Fig. 6. (a) The high resolution XPS scans over Bi 4f peaks of the Bi(1.0)/TiO_2 (rutile) photocatalyst for different visible light illumination time. (b) The high resolution XPS scans over Ti 2p peaks of the Bi(1.0)/TiO_2 (rutile) photocatalyst after visible light illumination. (c) The SPS measurement results of rutile TiO_2 nanoparticles and the Bi(1.0)/rutile photocatalyst.

rier separation and transfer behavior in the Bi(1.0)/TiO_2 (rutile) photocatalyst [43]. The magnitude of SPS response peak was dependent on the amount of net charge accumulated on the material surface [44]. Fig. 6c compares the SPS measurement results of rutile TiO_2 nanoparticles and the Bi(1.0)/TiO_2 (rutile) photocatalyst, which demonstrated clearly that much more holes were accumulated on rutile TiO_2 nanoparticles than on the Bi(1.0)/TiO_2 (rutile) photocatalyst because its positive SPS signal intensity was ~5 times than that of the Bi(1.0)/TiO_2 (rutile) photocatalyst. This observation also verified the hole trapping and consumption role of Bi quantum dots. Thus, it is no surprise that the photocatalytic reduction capability of rutile TiO_2 nanoparticles could be largely enhanced by the deposition of Bi quantum dots to trap and consume photogenerated holes. To further verify the hole trapping and consumption role of Bi quantum dots in this photocatalyst, the energy band alignment at the heterojunction interface of the Bi(1.0)/TiO_2 (rutile) photocatalyst was examined as detailed in the supplementary materials (see Fig. S3). The ΔE_{VBO} (valence band offset) and ΔE_{CBO} (conduction band offset) of the Bi(1.0)/TiO_2 (rutile) heterojunction were determined at 0.3 eV and 0.2 eV, respectively, which clearly demonstrated the metal to semiconductor transition happened in Bi quantum dots. Thus, photogenerated electrons by rutile TiO_2 under visible light illumination could not transfer from rutile TiO_2 to Bi quantum dots due to the energy band structure limitation, while photogenerated holes could migrate to Bi quantum dots.

4. Conclusions

In summary, Bi quantum dots were deposited on rutile TiO_2 nanoparticle surface to create the Bi/TiO_2 heterojunction photocatalyst. In this Bi/TiO_2 photocatalyst, rutile TiO_2 served as the main visible light absorber, while Bi quantum dots served as the hole trapping centers to enhance the charge carrier separation and eliminate the need of sacrificial agents to consume photogenerated holes in photocatalytic reduction process. Thus, an efficient photocatalytic bromate reduction under visible light illumination was achieved by this Bi/TiO_2 photocatalyst without the addition of sacrificial agents in the reaction solution, and it demonstrated a good regeneration capability and reusability. This study demonstrated a novel strategy for the design of photocatalysts with strong photocatalytic reduction capabilities for a broad range of technical applications.

Acknowledgements

This study was supported by the National Natural Science Foundation of China (Grant No. 51672283 and 51602316), the Basic Science Innovation Program of Shenyang National Laboratory for Materials Science (Grant No. Y4N56R1161 and Y5N56F2161), and the “Geping Green Action”-123 Project on Environment Research and Education of Liaoning Province (Grant No. CEPF2014-123-1-4).

Appendix A. Supplementary data

Supplementary data associated with this article can be found, in the online version, at http://dx.doi.org/10.1016/j.apcatb.2017.03.084.

References

[1] X. Zhao, H. Liu, Y. Shen, J. Qu, Appl. Catal. B: Environ. 106 (2011) 63–68.
[2] H. Noguchi, A. Nakajima, T. Watanabe, K. Hashimoto, Environ. Sci. Technol. 37 (2003) 153–157.

[3] A. Bhatnagar, Y. Choi, Y. Yoon, Y. Shin, B.-H. Jeon, J.-W. Kang, J. Hazard. Mater. 170 (2009) 134–140.
[4] H. Chen, Z. Xu, H. Wan, J. Zheng, D. Yin, S. Zheng, Appl. Catal. B: Environ. 96 (2010) 307–313.
[5] M. Chairez, A. Luna-Velasco, J.A. Field, X. Ju, R. Sierra-Alvarez, Biodegradation 21 (2010) 235–244.
[6] F. Chen, Q. Yang, Y. Zhong, H. An, J. Zhao, T. Xie, Q. Xu, X. Li, D. Wang, G. Zeng, Water Res. 101 (2016) 555–563.
[7] A. Fujishima, K. Honda, Nature 238 (1972) 37–38.
[8] M. Dahl, Y. Liu, Y. Yin, Chem. Rev. 114 (2014) 9853–9889.
[9] H. Park, H.-i. Kim, G.-h. Moon, W. Choi, Energy Environ. Sci. 9 (2016) 411–433.
[10] Y. Ma, X. Wang, Y. Jia, X. Chen, H. Han, C. Li, Chem. Rev. 114 (2014) 9987–10043.
[11] S.W. Verbruggen, J. Photochnol. Photobiol. C 24 (2015) 64–82.
[12] R. Marks, T. Yang, P. Westerhoff, K. Doudrick, Water Res. 104 (2016) 11–19.
[13] X. Huang, L. Wang, J. Zhou, N. Gao, Water Res. 57 (2014) 1–7.
[14] T. Peng, J. Tu, C. Hu, X. Hu, X. Zhou, J. Chem. Technol. Biotechnol. 89 (2014) 1425–1431.
[15] K.-Y.A. Lin, C.-H. Lin, S.-Y. Chen, H. Yang, Chem. Eng. J. 303 (2016) 596–603.
[16] D.Y.C. Leung, X. Fu, C. Wang, M. Ni, M.K.H. Leung, X. Wang, X. Fu, ChemSusChem 3 (2010) 681–694.
[17] S.N. Habisreutinger, L. Schmidt-Mende, J.K. Stolarczyk, Angew. Chem. Int. Ed. 52 (2013) 7372–7408.
[18] S.T. Kochuveedu, Y.H. Jang, D.H. Kim, Chem. Soc. Rev. 42 (2013) 8467–8493.
[19] X. Zhang, Y.L. Chen, R.-S. Liu, D.P. Tsai, Rep. Prog. Phys. 76 (2013) 046401–046442.
[20] H.B. Michaelson, J. Appl. Phycol. 48 (1977) 4729–4733.
[21] S. Kim, S.-J. Hwang, W. Choi, J. Phys. Chem. B 109 (2005) 24260–24267.
[22] Y.-M. Lin, X. Sun, M.S. Dresselhaus, Phys. Rev. B 62 (2000) 4610–4623.
[23] N.A. Kouame, O.T. Alaoui, A. Herissan, E. Larios, M. Jose-Yacaman, A. Etcheberry, C. Colbeau-Justin, H. Remita, New J. Chem. 39 (2015) 2316–2322.
[24] S. Weng, B. Chen, L. Xie, Z. Zheng, P. Liu, J. Mater. Chem. A 1 (2013) 3068–3075.
[25] F. Dong, Q. Li, Y. Sun, W.-K. Ho, ACS Catal. 4 (2014) 4341–4350.
[26] X. Liu, H. Cao, J. Yin, Nano Res. 4 (2011) 470–482.
[27] J. Schneider, M. Matsuoka, M. Takeuchi, J. Zhang, Y. Horiuchi, M. Anpo, D.W. Bahnemann, Chem. Rev. 114 (2014) 9919–9986.
[28] F. Qin, G. Li, H. Xiao, Z. Lu, H. Sun, R. Chen, Dalton Trans. 41 (2012) 11263–11266.
[29] L. Yanhong, W. Dejun, Z. Qidong, Y. Min, Z. Qinglin, J. Phys. Chem. B 108 (2004) 3202–3206.
[30] Y. Xu, M.A.A. Schoonen, Am. Miner. 85 (2000) 543–556.
[31] D.O. Scanlon, C.W. Dunnill, J. Buckeridge, S.A. Shevlin, A.J. Logsdail, S.M. Woodley, C.R.A. Catlow, M.J. Powell, R.G. Palgrave, I.P. Parkin, G.W. Watson, T.W. Keal, P. Sherwood, A. Walsh, A.A. Sokol, Nat. Mater. 12 (2013) 798–801.
[32] D. Velasco-Arias, I. Zumeta-Dubé, D. Díaz, P. Santiago-Jacinto, V.-F. Ruiz-Ruiz, S.-E. Castillo-Blum, L. Rendón, J. Phys. Chem. C 116 (2012) 14717–14727.
[33] X. Zhang, T. Zhang, J. Ng, J.H. Pan, D.D. Sun, Environ. Sci. Technol. 44 (2010) 439–444.
[34] H. Li, Z. Bian, J. Zhu, Y. Huo, H. Li, Y. Lu, J. Am. Chem. Soc. 129 (2007) 4538–4539.
[35] U.W. Hamm, D. Kramer, R.S. Zhai, D.M. Kolb, Electrochim. Acta 43 (1998) 2969–2978.
[36] J. Hou, C. Yang, Z. Wang, S. Jiao, H. Zhu, Appl. Catal. B: Environ. 129 (2013) 333–341.
[37] F. Dong, T. Xiong, Y. Sun, Z. Zhao, Y. Zhou, X. Feng, Z. Wu, Chem. Commun. 50 (2014) 10386.
[38] S.O. Saied, J.L. Sullivan, T. Choudhury, C.G. Pearce, Vacuum 38 (1988) 917–922.
[39] J. Tauc, R. Grigorovici, A. Vancu, Phys. Stat. Sol. (B) 15 (1966) 627–637.
[40] J. Toudert, R. Serna, M. Jiménez de Castro, J. Phys. Chem. C 116 (2012) 20530–20539.
[41] R. Li, Y. Weng, X. Zhou, X. Wang, Y. Mi, R. Chong, H. Han, C. Li, Energy Environ. Sci. 8 (2015) 2377–2382.
[42] Y. Ma, X. Wang, C. Li, Chinese J. Catal. 36 (2015) 1519–1527.
[43] V. Duzhko, V.Y. Timoshenko, F. Koch, T. Dittrich, Phys. Rev. B 64 (2001) 075204.
[44] Q. Zhang, D. Wang, J. Xu, J. Cao, J. Sun, M. Wang, Mater. Chem. Phys. 82 (2003) 525–528.